

ARTICLE

<https://doi.org/10.1038/s41467-019-08459-9>

OPEN

Emergence of a field-driven $U(1)$ spin liquid in the Kitaev honeycomb model

Ciarán Hickey¹ & Simon Trebst¹

In the field of quantum magnetism, the exactly solvable Kitaev honeycomb model serves as a paradigm for the fractionalization of spin degrees of freedom and the formation of \mathbb{Z}_2 quantum spin liquids. An intense experimental search has led to the discovery of a number of spin-orbit entangled Mott insulators that realize its characteristic bond-directional interactions and, in the presence of magnetic fields, exhibit no indications of long-range order. Here, we map out the complete phase diagram of the Kitaev model in tilted magnetic fields and report the emergence of a distinct gapless quantum spin liquid at intermediate field strengths. Analyzing a number of static, dynamical, and finite temperature quantities using numerical exact diagonalization techniques, we find strong evidence that this phase exhibits gapless fermions coupled to a massless $U(1)$ gauge field. We discuss its stability in the presence of perturbations that naturally arise in spin-orbit entangled candidate materials.

¹Institute for Theoretical Physics, University of Cologne, 50937 Cologne, Germany. Correspondence and requests for materials should be addressed to C.H. (email: chickey@thp.uni-koeln.de)

Quantum spin liquids are highly entangled quantum states of matter that exhibit fractionalized excitations¹. A principle example for such a fractionalization are the spinon excitations of a resonating valence bond (RVB) liquid², which carry spin-1/2 and arise only after breaking apart a spin-1 excitation originating from an elementary spin-flip process. Crucially, once a pair of spinons has been created in an RVB liquid, they can be separated to arbitrary distances at no energy cost—the spinons are deconfined. This reveals the emergence of a much larger underlying structure present in any quantum spin liquid—a lattice gauge theory in its deconfined regime. The interplay of fractionalization and lattice gauge theory can be conceptualized by a parton construction³, which decomposes the original spin degrees of freedom in terms of partons that represent the emergent fractional degrees of freedom. These partons can be chosen to be complex Abrikosov fermions⁴, real Majorana fermions^{5,6}, or bosons. Concomitantly, the system is found to be enriched by an emergent gauge structure, with examples including continuous $U(1)$ or discrete \mathbb{Z}_2 gauge symmetry^{7,8}. One of the most beautiful examples of a parton construction has been introduced by Kitaev, who was able to devise an exactly solvable spin-1/2 model on the honeycomb lattice with several quantum spin liquid ground states⁶. Here, the fractionalization of the original spin degrees of freedom into Majorana fermions and an emergent \mathbb{Z}_2 gauge structure naturally appear in the framework of Kitaev's exact solution, which has led to a plethora of theoretical investigations and deep analytical insights into spin liquid physics⁹.

On a microscopic level, the key ingredients of the Kitaev model are its bond-directional Ising-type exchange interactions. Remarkably, these seemingly unusual interactions are found to be realized via an intricate interplay of spin-orbit coupling, crystal field effects, and strong interactions^{10,11} in a variety of $4d$ and $5d$ materials¹². However, these spin-orbit entangled Mott insulators are typically found to exhibit ordered states at low temperatures in lieu of the sought-after spin liquid physics, consistent with a theoretical analysis of perturbed Kitaev magnets that exhibit more conventional types of exchanges beyond a dominant bond-directional interaction^{13–20}.

Recently considerable excitement has arose due to the fact that in one of these materials, RuCl_3 , the magnetic order can be suppressed with an in-plane magnetic field^{21–28}. Probably the most spectacular result is a report²⁹ for tilted field directions, which suggests that a phase, intermediate between the magnetically ordered state at low fields and the high-field polarized state, exhibits a half-quantized thermal Hall conductance—a unique signature for a gapped topological spin liquid. The precise nature of the putative quantum spin liquid regime and its microscopic description, however, still remain open.

Here, motivated by these observations, we return to the original Kitaev model and explore its phase diagram in the presence of tilted magnetic fields using numerical exact diagonalization (ED) techniques. As we report in this Article, there are two distinct spin liquid regimes already present in this model. For small magnetic field strengths, there is a gapped spin liquid phase whose non-Abelian topological nature has first been rationalized by Kitaev using perturbative arguments for a field pointing along the out-of-plane $[111]$ direction⁶. Here we demonstrate that this phase is stable when tilting the magnetic field to generic directions and well beyond the perturbative regime by explicitly calculating the modular S -matrix from its (quasi-)degenerate ground states, which unambiguously confirms that its inherent topological nature is indeed given by the Ising topological quantum field theory (TQFT). The second spin liquid, on which we focus in this Article, is both manifestly distinct from the gapped topological spin liquid and at the same time can be considered, in many ways,

to be a descendent of it. One key distinction between the two phases is their underlying gauge structure. While the Kitaev spin liquid is accompanied by a \mathbb{Z}_2 gauge structure with gapped vison excitations in the gauge sector, the second spin liquid is found to exhibit the gapless gauge structure typically associated with a $U(1)$ spin liquid.

Results

Overview. In what follows, we provide multi-faceted evidence that the phase transition between the two spin liquids at finite field strengths is driven by the closing of the gap for vison excitations of the \mathbb{Z}_2 spin liquid and that the emergent gapless spin liquid is a $U(1)$ spin liquid with a spinon Fermi surface, by investigating the evolution of the energy spectrum, the dynamical structure factor, and thermodynamic signatures in the specific heat. We discuss aspects of the underlying field theory governing this phase transition at the end of the Article.

It should be noted that the occurrence of two stable spin liquid regimes in the Kitaev model exposed to a (tilted) magnetic field is closely linked to whether the applied field matches the underlying antiferromagnetic (AFM) or ferromagnetic (FM) spin correlations, with an order of magnitude difference in the critical fields between the two cases. Only for AFM Kitaev couplings and a uniform magnetic field, do we observe the two spin liquids discussed above. For FM Kitaev couplings the gapped Kitaev spin liquid is found to be considerably less stable than in the AFM case, consistent with a number of recent numerical studies^{30–32} (with ref. ³¹ also the first to report the existence of an intermediate phase for an AFM coupling). Notably, this situation can be reversed by staggering the magnetic field, which dramatically increases the stability of the FM Kitaev phase, while the AFM spin liquid then covers a significantly smaller parameter space. To round off our discussion, we demonstrate the stability of the emergent gapless spin liquid when perturbing the Kitaev model with a conventional Heisenberg interaction or an off-diagonal Γ -exchange, which constitute further ingredients of the microscopic description of Kitaev materials¹⁷.

Model. We start our discussion by considering the pure Kitaev honeycomb model in the presence of a uniform magnetic field of arbitrary orientation, defined by the Hamiltonian

$$H_{\pm} = \pm K \sum_{\langle ij \rangle \in \gamma} S_i^{\gamma} S_j^{\gamma} - \sum_i \mathbf{h} \cdot \mathbf{S}_i, \quad (1)$$

where H_{\pm} indicates an AFM/FM Kitaev coupling and the bond directions are denoted by $\gamma \in \{x, y, z\}$. We parametrize the orientation of the magnetic field as $\mathbf{h} = h \sin \theta \hat{\mathbf{h}}_{111} + h \cos \theta \hat{\mathbf{h}}_{\perp}$, where the unit vectors $\hat{\mathbf{h}}_{111}$ and $\hat{\mathbf{h}}_{\perp}$ point along the $[111]$ and either $[11\bar{2}]$ or $[\bar{1}10]$ directions. For materials such as $(\text{Na}, \text{Li})_2\text{IrO}_3$ and RuCl_3 these directions correspond to the out-of-plane, c -axis, and in-plane, a or b -axes, respectively. The angle θ thus measures the tilt away from the honeycomb planes.

Phase diagrams. The phase diagram of the model for various tilt angles of a uniform external magnetic field is presented in Fig. 1 for both the AFM and FM Kitaev cases. The phase boundaries, presented in this Figure, are based on a number of different signatures, including the second derivative of the ground-state energy and the ground-state fidelity (see Methods for more details). There are certain limits which have previously been discussed:

- (i) $h = 0$. In the case of zero magnetic field the Kitaev Hamiltonian is exactly solvable⁶. Following Kitaev's

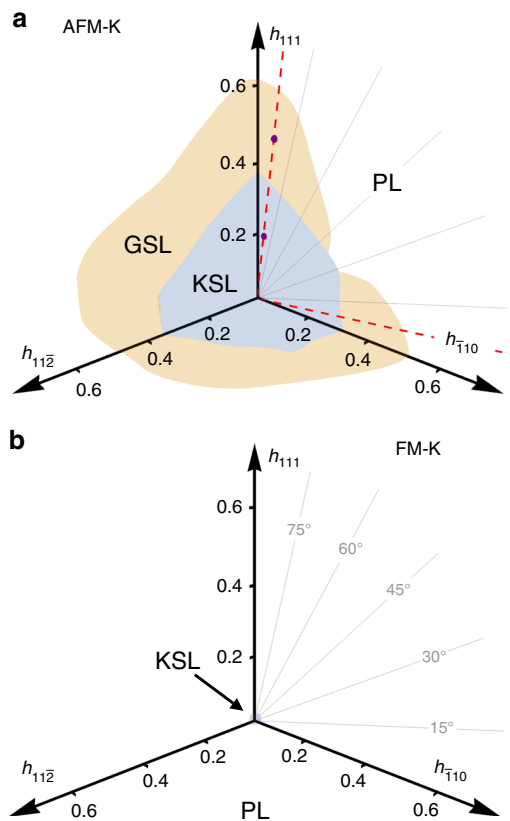


Fig. 1 Phase diagrams in a uniform magnetic field. **a** The pure AFM Kitaev model and **b** the pure FM Kitaev model for various tilt angles. For AFM couplings the gapped Kitaev spin liquid (KSL) is surrounded, for a wide range of tilt angles, by a gapless spin liquid (GSL) before giving way to a trivial polarized state (PL). For FM couplings, in contrast, the KSL is found to cover a considerably smaller parameter region with no intermediate GSL (see Supplementary Note 1 for a zoomed-in view of the FM phase diagram). The two (purple) points in **(a)** mark the parameters at which the dynamical structure factor in Fig. 4b, c is plotted

original solution, each spin-1/2 can be split into four Majorana fermions, three are associated with the adjacent bonds and one with the original site. The bond Majoranas can be recombined to form a static \mathbb{Z}_2 gauge field, leaving us with a single free Majorana fermion moving in a background field. Its spectrum is gapless, with Dirac points located at the corners of the Brillouin zone, while the vison excitations of the gauge field remain gapped^{6,9}. The net result is a gapless \mathbb{Z}_2 spin liquid.

- (ii) $h \parallel [111]$, $h \ll K$. In the presence of a magnetic field along the $[111]$ direction, Kitaev showed, using perturbation theory, that a small field opens up a gap in the Majorana spectrum. Furthermore, the resulting Majorana insulator has a non-trivial band structure, with a Chern number $C = 1$ for the lower, fully filled band. This corresponds to a gapped non-Abelian spin liquid with Ising anyon topological order, which we will refer to as the Kitaev spin liquid (KSL). The gapped flux excitations (visons) now bind a Majorana fermion and there is a single chiral gapless Majorana edge mode, which gives rise to a quantized thermal quantum Hall effect. Our numerical data confirms that this scenario remains true away from the perturbative limit, for generic field directions, and applies to both the AFM and FM cases. Technically, we do so by calculating³³ the modular S -matrix from the three (quasi-)degenerate

ground states in the KSL phase for various parameters of Fig. 1. The entries S_{ab} encode the braiding properties of quasiparticles a and b in the underlying TQFT (fixing the entries to certain universal values) and thereby allow for its unambiguous identification. Numerically, we find, e.g., the following S -matrix

$$S_{\text{ED}} = \begin{pmatrix} 0.46 & 0.74 & 0.47 \\ 0.71 & 0.04e^{-0.91i} & -0.70 \\ 0.49 & -0.67e^{0.02i} & 0.58e^{-0.13i} \end{pmatrix}, \quad (2)$$

computed for a $[111]$ field of magnitude $h \sim h_{\text{KSL}}^{\text{crit}}/2$. For the Ising TQFT the expected S -matrix has corner entries $\pm 1/2$, a middle entry of zero, and the remaining four entries $\pm 1/\sqrt{2}$. We see that, even for the $N=24$ site cluster at hand, we are able to numerically resolve this structure, confirming that the KSL is indeed a non-Abelian quantum spin liquid described by an Ising TQFT.

- (iii) $h \gg K$. For sufficiently large magnetic field the system will clearly become polarized along the axis of the external field. In this polarized phase (PL) the ground state is a trivial product state and the lowest energy excitations are conventional magnon modes.

The phase diagrams of Fig. 1 expand this perspective by providing the critical field strengths, at which the KSL is destroyed, for tilted field setups. As can be seen in Fig. 1, the critical field does not depend sensitively on the field direction (though in real materials anisotropic g -factors need to be considered that will distort the phase diagram). What is strikingly evident, however, is that there is a marked contrast in the stability of the KSL in the case of AFM versus FM coupling, with an order of magnitude difference in the critical fields. To investigate the source of this difference we show in Fig. 2 the phase diagrams for a staggered external field, with $+\mathbf{h}$ applied on one sublattice and $-\mathbf{h}$ on the other sublattice of the honeycomb lattice. We see that, in this case, there is still an order of magnitude difference in the critical fields but now the situation has been reversed. The AFM KSL is significantly less stable in a staggered field compared to a uniform one, while the FM KSL is less stable in a uniform field and significantly more stable in a staggered one. The stability of the KSL thus crucially depends on whether the applied field matches the underlying spin correlations or not. We expect this observation to generically hold and to also apply to the three-dimensional generalizations of the Kitaev model³⁴ under an external field. Though it is experimentally not possible to generate a staggered field using conventional magnets, it may be possible to realize the desired effect by placing thin samples of a Kitaev material on a substrate which is a trivial honeycomb antiferromagnet, producing a staggered field by proximity, and thereby allowing to probe this effect.

Intermediate gapless phase. Beyond the KSL there is, for a wide range of field angles in the case of AFM Kitaev couplings, an intermediate phase before entering the high-field PL state. To investigate the properties of this phase we focus on two generic cuts away from any high-symmetry directions, shown by the dashed (red) lines in Fig. 1, one close to the in-plane $[\bar{1}10]$ direction at $\theta = 7.5^\circ$ ($\pi/24$) and the other close to the out-of-plane $[111]$ direction at $\theta = 82.5^\circ$ ($11\pi/24$) (for an example of a cut in which there is a single, direct KSL-PL transition see Supplementary Note 2).

One striking signature for the transition from the KSL to this intermediate phase is a dramatic increase in the density of states at low energies. This is illustrated in Fig. 3a, b, which show the full low-energy spectrum as a function of increasing field magnitude

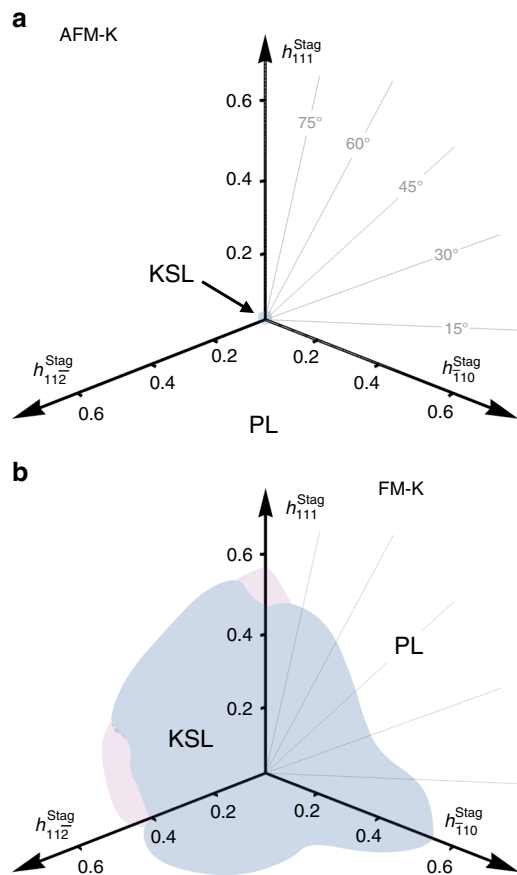


Fig. 2 Phase diagrams in a staggered magnetic field. **a** The pure AFM Kitaev model and **b** the pure FM Kitaev model. The pink shading marks a region of potential interest (not explored here)

(obtained from numerical exact diagonalization) for the two cuts, with states labeled by their momentum quantum number. Indeed, for the energy window shown here there are more than 10 times as many states within the intermediate phase as there are in the zero-field Kitaev limit. This increase of the low-energy density of states by more than an order of magnitude (in combination with no degenerate ground-state manifold) is a strong indication that the intermediate phase is in fact a gapless phase with considerably more low-energy modes than the gapless KSL in the vanishing field limit. This incredible density of states at low energies is supported by finite-size scaling, shown in the Methods section, making it a robust feature of the intermediate phase. Beyond the intermediate phase, we see that this plethora of low-lying states quickly get pushed up linearly, consistent with the notion that a spin gap begins to open upon the transition to the PL state.

To probe the magnetic nature of this intermediate gapless phase, we turn to the static spin structure factor of the ground state, $S(\mathbf{q}) = \frac{1}{N} \sum_{ij} \langle \mathbf{S}_i \cdot \mathbf{S}_j \rangle e^{i\mathbf{q} \cdot (\mathbf{r}_i - \mathbf{r}_j)}$, which is plotted in Fig. 3c, d for the two cuts. There are no clear signs of any magnetic ordering, with only the Γ point intensity (i.e., the magnetization) significantly changing as the transition from the KSL to the intermediate phase is crossed. The flat, rather featureless structure factor of the intermediate phase is indicative of a quantum spin liquid phase. We also show the flux of the \mathbb{Z}_2 gauge field through the plaquettes of the honeycomb lattice, $\langle W \rangle_P = \langle S_i^x S_j^y S_k^z S_l^x S_m^y S_n^z \rangle$, in Fig. 3e, f. This quantity does not show visible signatures of the transitions. The flux $\langle W \rangle_P \approx 1$ in the KSL phase and $\langle W \rangle_P \approx 0$ in the PL phase. In the intermediate phase it takes a range of

intermediate values, interpolating between these two limits. This indicates that the plaquette flux is heavily fluctuating in the intermediate phase. Taken together, all of these results are consistent with a gapless, disordered state, allowing us to identify the intermediate phase as a gapless spin liquid (GSL).

This immediately raises the question about the origin and nature of the gapless degrees of freedom. To answer this question it has proved particularly insightful to look at the dynamical spin structure factor, which provides strong indications that it is the vison gap which closes at the transition to the intermediate gapless phase. The dynamical spin structure can be written in Lehmann representation as

$$S^{\alpha\alpha}(\mathbf{Q}, \omega) = \sum_n |\langle n | S_{\mathbf{Q}}^{\alpha} | 0 \rangle|^2 \delta(\omega - (E_n - E_0)), \quad (3)$$

where we note that the $n=0$ contribution, which, for $\mathbf{Q}=\Gamma$, is simply $|\langle S_{\text{total}}^{\alpha} \rangle|^2$, the magnetization induced by the external field, is not included in the following discussion. Furthermore, from now on, we will focus on the sum $S(\mathbf{Q}, \omega) = \sum_{\alpha} S^{\alpha\alpha}(\mathbf{Q}, \omega)$. At zero field there is, despite the system being gapless in this limit, a distinct gap to physical spin excitations as these involve the creation of gapped \mathbb{Z}_2 flux excitations^{35,36}. This flux gap is clearly visible in Fig. 4a, with its uniformity across momenta reflecting the static nature of the flux excitations. Note that the flux gap is absent at the Γ point for the AFM Kitaev model due to the AFM correlations of the ground state. Upon applying the magnetic field, this uniform flux gap breaks apart and a significant portion of the spin spectral weight is pushed to zero energy across the whole Brillouin zone as illustrated in Fig. 4b for a point midway in the KSL phase along the cut at $\theta=82.5^\circ$. These states are further pushed down in energy as the transition to the intermediate phase is crossed, with Fig. 4c showing results for a point in the middle of the intermediate phase. The overall spin spectral weight of these low-energy states makes up a significant part (~40%) of the zero-field flux gap. This is strong evidence that the transition from the KSL to the intermediate phase is thus marked by the closure of the flux gap (see Supplementary Note 3 for further discussion of the flux gap closure for the cut at $\theta=7.5^\circ$). In the intermediate phase the dynamical structure factor at higher energies remains featureless, with weight distributed across all energies. There are no signatures of pseudo-Goldstone modes or any kind of conventional magnon excitations. These features support the case for a gapless quantum spin liquid arising from the closing of the \mathbb{Z}_2 flux gap.

The key role played by the flux excitations is also visible at finite temperatures. In Fig. 5 we show the specific heat as a function of increasing field, calculated using the method of thermal pure quantum states^{37,38}. At zero field, it has been established through numerical exact Monte Carlo simulations³⁹ that there are two finite temperature crossovers, a high-temperature one associated with the itinerant Majorana fermions indicating the fractionalization of the original spins and a low-temperature one associated with the \mathbb{Z}_2 gauge field, at which it orders into its ground-state configuration. The location of these peaks is correlated to the bandwidth of the fermion hopping and the vison gap in the gauge sector respectively. As one approaches the transition to the intermediate phase the low- T peak starts to drift to lower and lower temperatures. This is another telling sign that the energy scale associated with the gauge field is lowered as the field increases. Interestingly, the high- T peak does not show any notable changes as the transition to the intermediate phase is crossed. This would seem to suggest that the itinerant Majoranas are not affected by the transition, with all of the action occurring only in the gauge sector. Once the PL phase is entered a single peak develops, as expected since fractionalization is lost.

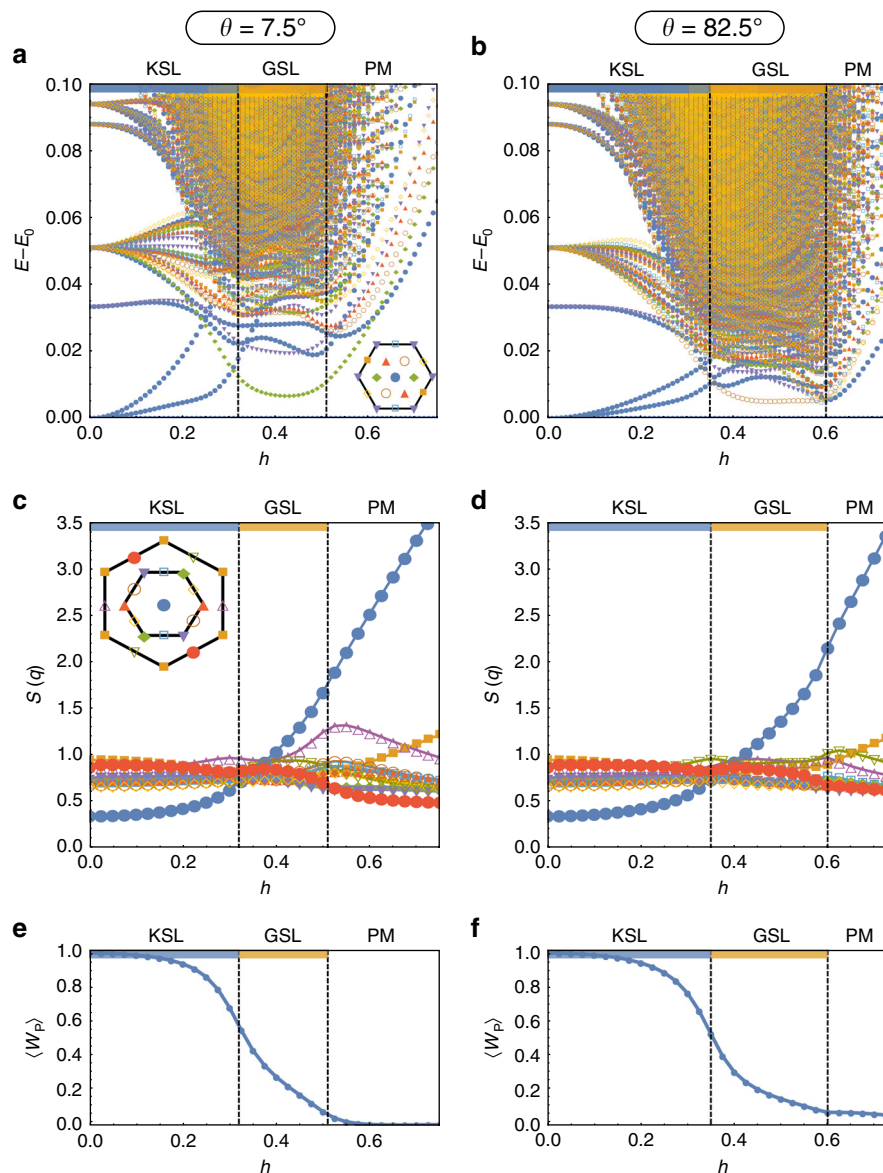


Fig. 3 Energy spectrum, static spin structure factor, and plaquette flux. In **a–c** a cut through the pure AFM Kitaev phase diagram at an angle of $\theta = 7.5^\circ$ and in **d–f** at $\theta = 82.5^\circ$. These cuts correspond to the red dashed lines in Fig. 1a

Beyond the Kitaev model. Before turning to a discussion of the nature of the intermediate gapless spin liquid phase, we round off our numerical results with a study of its stability in the presence of microscopic perturbations. In any Kitaev material, the bond-directional exchanges of the Kitaev model are accompanied by other, more conventional, interactions such as symmetric off-diagonal exchange terms (Γ -interactions) along with an isotropic Heisenberg coupling^{12,17,19}. In Fig. 6, we illustrate phase diagrams elucidating the effects of these additional couplings in the vicinity of the pure Kitaev model for various tilt angles of the magnetic field. It is clear that the intermediate GSL is stable under both kinds of perturbations. Indeed the stability of the GSL mirrors that of the KSL, always sitting above it in these phase diagrams. This suggests that the intermediate phase is in fact a descendent of the KSL, resulting from an instability of the gapped Ising anyon phase.

Discussion

To summarize our key results, we have established that the Kitaev honeycomb model contains another phase exhibiting

unconventional magnetism alongside its already well-known gapless and gapped \mathbb{Z}_2 spin liquid phases. This additional phase is gapless with a dense continuum of excitations, featureless structure factor (both static and dynamic), fluctuating \mathbb{Z}_2 fluxes, and low-energy spin spectral weight.

To reveal the precise nature of this phase the central question is what its gapless degrees of freedom are—matter or gauge fields or both? Though this question is difficult to answer definitively, we interpret our results as providing multi-faceted evidence for the emergence of a $U(1)$ spin liquid, in which gapless fermions are coupled to a massless gauge field. Our conclusion is guided by the following observations.

First, the energy spectrum shows that the transition from the KSL to the GSL occurs through the dramatic shift of a large density of states to low energies, forming a dense continuum of gapless excitations. The dynamical structure factor reveals that these states carry with them physical spin spectral weight at all momenta. Since we know from exact studies at zero field that only the vison excitations of the KSL (but not the Majorana fermions) carry spin spectral weight, this indicates, supported also

the paragraphs below give an interpretation of the phase shown in Fig. 3e

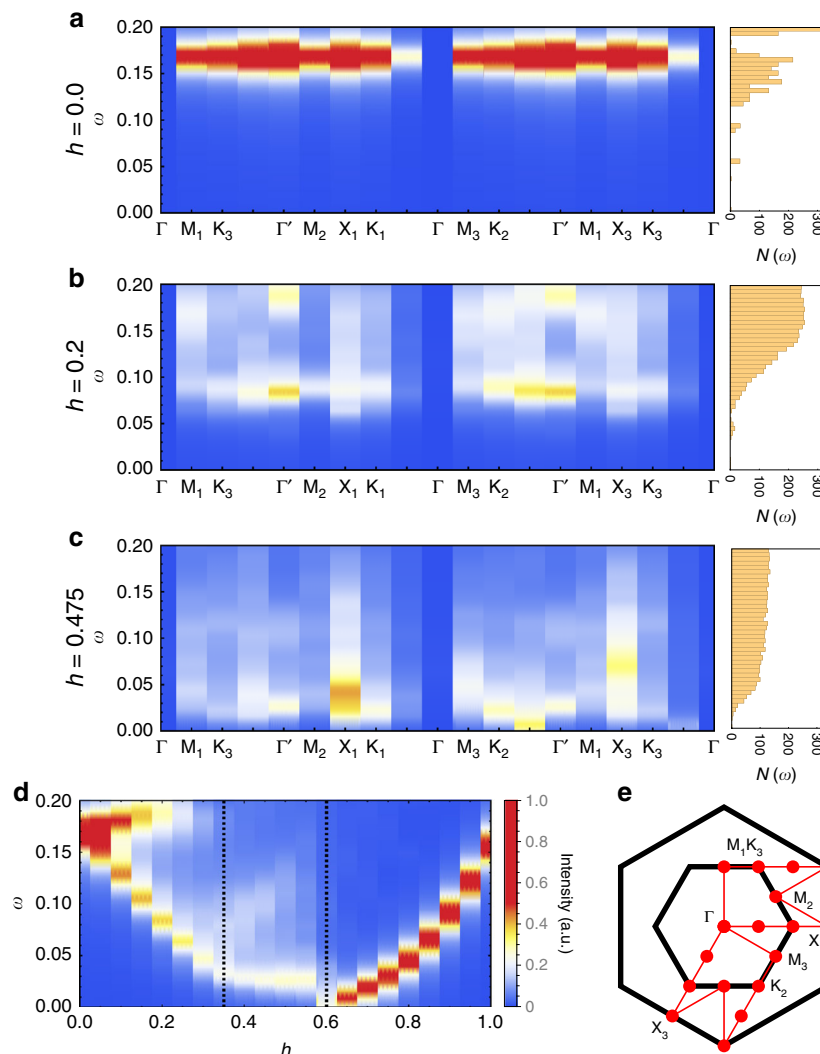


Fig. 4 Dynamical spin structure factor. **a** The zero-field KSL, **b** a point midway in the KSL phase, and **c** a point in the middle of the GSL along a path through all high-symmetry points of the extended Brillouin zone as illustrated in **(e)**. In **d**, the intensity at the Γ' point is shown as a function of increasing field along the cut $\theta = 82.5^\circ$, the upper of the two dashed red lines in Fig. 1a

by the thermodynamic signatures in the specific heat, that this transition is marked by the closing of the vison gap, resulting in a massively fluctuating gauge field. Naively, one could identify this gap closing with vison condensation which in turn should lead to confinement and a trivial, magnetically ordered phase (such as the transition from the KSL to zig-zag magnetic ordering in the presence of additional Heisenberg interactions¹⁶). However, in the KSL, the visons carry a Majorana mode (which is the hallmark of its topological order) and so cannot condense by themselves. If the visons indeed avoid condensation at the gap closing transition, this leads to an intriguing scenario in which their associated Majorana fermions form a gapless Fermi surface coupled to a massless gauge field.

Second, a particularly enlightening and intuitive perspective on the transition to the GSL can be gained by considering an alternative Abrikosov fermionic parton decomposition of the spin operators. Such partons naturally possess an accompanying $U(1)$ gauge structure. If we imagine starting from a phase in which the fermionic partons, coupled to such a $U(1)$ gauge field, form a Fermi surface the KSL can naturally be accessed through a pairing instability of the fermions^{40,41}. The formation of a superconducting condensate Higgses the gapless $U(1)$ gauge field down to a gapped \mathbb{Z}_2 gauge field. In order to properly match the

topological properties of the KSL, the superconductor must be a chiral p -wave superconductor, which ensures, for example, that flux excitations can bind Majorana fermions⁴². Starting from zero field, we see that, in this picture, the transition from the KSL to the intermediate GSL can be understood as a transition from a gapped chiral p -wave superconductor, coupled to a gapped \mathbb{Z}_2 gauge field, to a gapless spinon Fermi surface, coupled to an emergent $U(1)$ gauge field. The Fermi surface can be stabilized by a lack of lattice symmetries and momentum conservation⁴³.

The key to the realization of this scenario in the present context is that we can have an emergent $U(1)$ conservation of the fermionic partons, with the closure of the vison gap thus related to the emergence of this conservation law. The Majoranas remain intact throughout the transition, with the only change being that, in the GSL, the Majoranas can now be combined into complex fermions with an emergent $U(1)$ particle conservation. This naturally explains why the Majorana peak in the specific heat is relatively unaffected as the transition to the GSL is crossed.

The transition from the GSL to the PL phase can be similarly understood within this framework, corresponding to a transition from a gapless Fermi surface to a gapped trivial insulator. With the fermions completely gapped, they can be integrated out to produce a low-energy theory of a pure compact $U(1)$ gauge

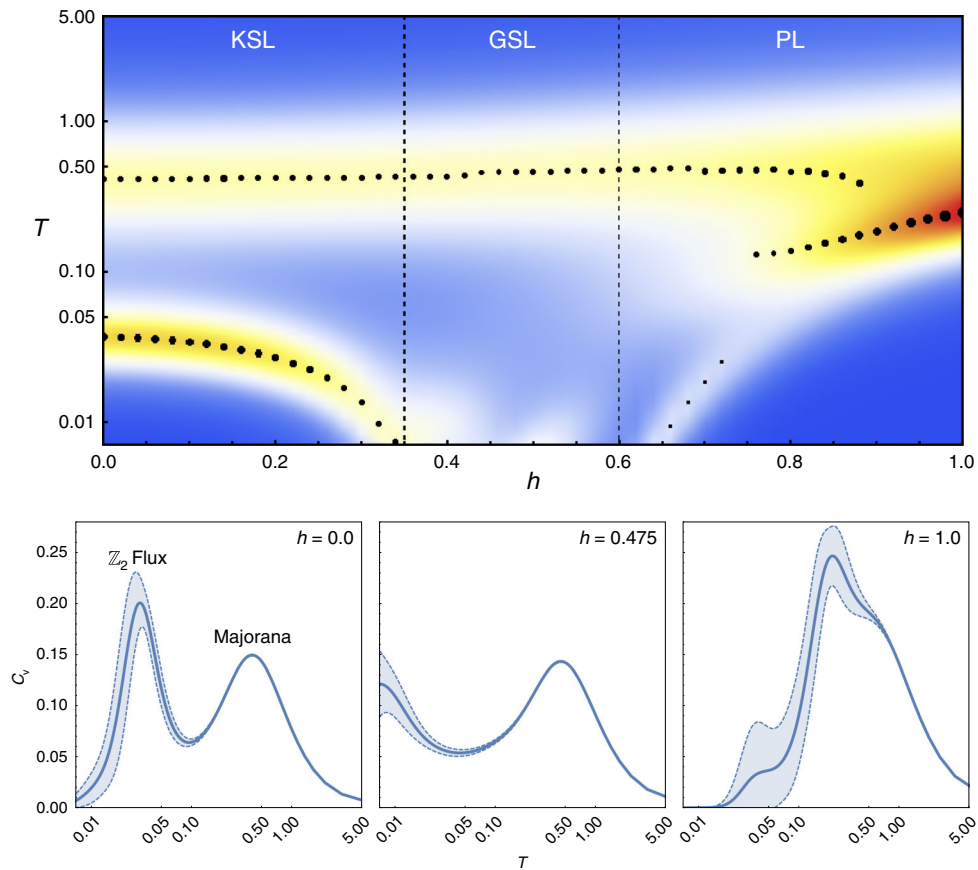


Fig. 5 Specific heat as a function of temperature for increasing field. Shown along the cut at $\theta = 82.5^\circ$ (upper panel). The black circles (and their widths) indicate the location (and heights) of the maxima. The three lower panels show specific heat scans for the zero-field KSL, the intermediate GSL at $h = 0.475$ (note that though it is not shown here, the specific heat goes to zero as $T \rightarrow 0$), and the PL state at $h = 1.0$, respectively. The light blue shading indicates the standard deviation of the estimates

theory. However, such a theory is well-known to be unstable to confinement via monopole proliferation^[50], resulting in a completely trivial gapped phase, the PL phase. The complex Abrikosov fermion perspective thus naturally gives an intuitive and unified description of all of the numerical data at hand. This is summarized in Fig. 7 in which the behavior of the gauge field and fermionic partons in the KSL, GSL and PL phases is detailed.

This parton perspective also motivates a natural field theory description of the transition from the KSL to the GSL in terms of a Fermi surface of partons coupled to a dynamical $U(1)$ gauge field

$$\mathcal{L} = \psi^\dagger \left(D_t - \frac{1}{2m} D_i^2 - \mu \right) \psi + g(\psi^\dagger \Delta \psi^\dagger + h.c.) + \dots, \quad (4)$$

where ψ represent the low-energy fermionic parton modes near the Fermi surface, $D_\mu = i\partial_\mu + a_\mu$, $\Delta = |\Delta|(\partial_x \pm i\partial_y)$ corresponds to a decoupling in the chiral p-wave channel of an attractive four-fermion interaction of strength g and the higher order terms include a kinetic term for the dynamical gauge field a . For $\Delta = 0$ we have a Fermi surface of partons coupled to a dynamical $U(1)$ gauge field. This corresponds to the GSL phase. Though normally one might expect such a Fermi surface to be immediately susceptible to a pairing instability, here we have an extended phase, with the Fermi surface stable up to a finite critical strength of the attractive interaction⁴⁰ and further stabilized by the lack of lattice symmetries and momentum conservation discussed above (see Supplementary Note 4 for further discussion). At the transition pairing onsets, such that for $\Delta \neq 0$ the fermions become gapped

and can be integrated out. If the gapped fermions occupy a topologically non-trivial band structure this will generate a Chern-Simons term at level 1/2, ensuring that in vortex cores (where the superconducting condensate vanishes) there is a bound Majorana fermion⁴², and a mass term for the gauge field generated by the Anderson-Higgs mechanism. This corresponds to the KSL phase. This simple, minimal theory is thus able to capture the physics either side of the transition.

Last, let us mention, for completeness, an alternative scenario for the transition between the KSL and GSL. The scenario, which we can definitively rule out based on our numerical data, starts from the KSL and argues^{44,45} that instabilities of this topological phase can be driven by the condensation of Ising anyons, which are brought into close proximity with increasing field strength. However, the ensuing phase is still a chiral spin liquid (albeit with an Abelian topological order) which would reveal itself through a ground-state degeneracy that we do not observe in our numerical data for the GSL (in contrast to the KSL where the threefold quasi-degenerate ground states strongly corroborate its topological nature via the S-matrix calculation showcased above).

In conclusion, our numerical analysis of the complete phase diagram of the Kitaev model in tilted magnetic fields has revealed that this fundamental model harbors not only \mathbb{Z}_2 spin liquid physics, but also exhibits an extended spin liquid regime with a distinct $U(1)$ gauge structure. Our numerical observation of the phase transition between these two regimes at finite field strengths provides a multi-faceted perspective of the accompanying signatures in static, dynamical, and finite temperature quantities. It will be an interesting avenue for future theoretical

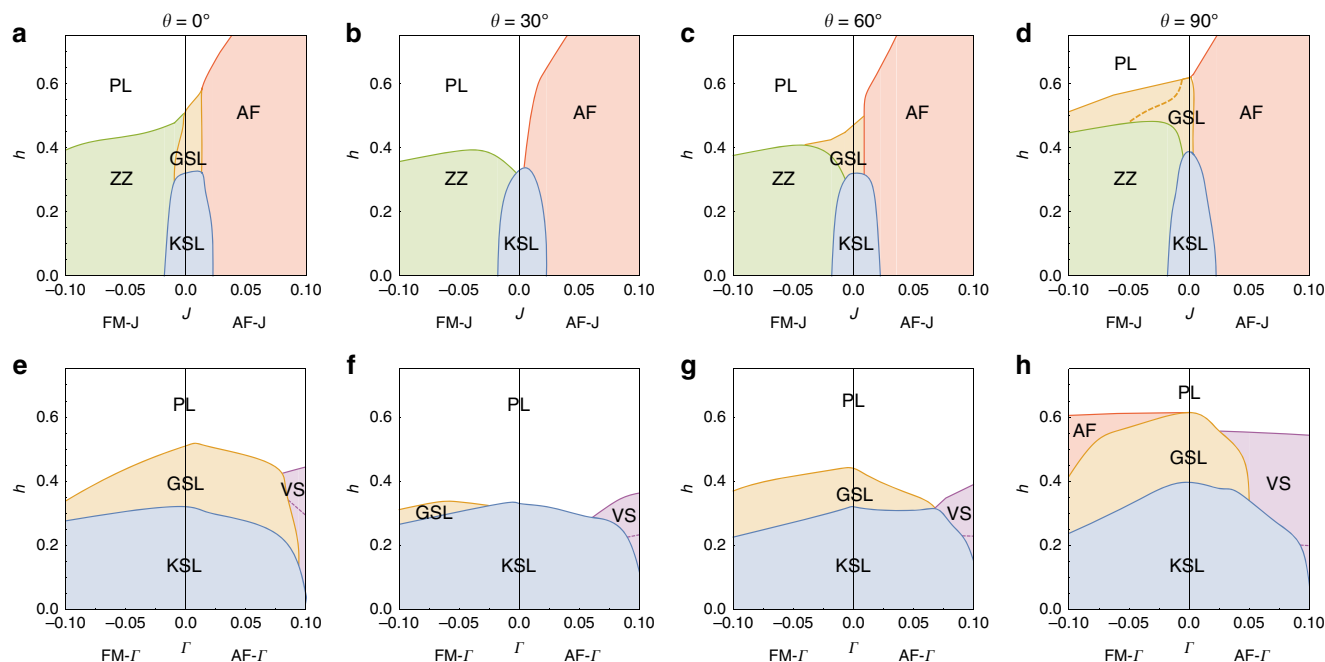


Fig. 6 Phase diagrams beyond the pure Kitaev model. Effects of **a–d** an additional Heisenberg and **e–h** an additional off-diagonal Γ exchange on the KSL and GSL in tilted magnetic fields. The Kitaev interaction is parameterized by α and the perturbing coupling by $(1 - \alpha)/2$, with $\alpha = 1$ corresponding to the pure Kitaev model and $\alpha = 0.8$ to the edges of the phase diagram, $J = \pm 0.1$, $\Gamma = \pm 0.1$. In the presence of additional Heisenberg interactions both spin liquid phases eventually give way to either zig-zag (ZZ) or antiferromagnetic (AF) ordering. The inclusion of the additional off-diagonal Γ -exchange affects the stability of the spin liquid phases in a lesser way, with AF or vortex state (VS) order arising only for large coupling strengths. Note that in all phase diagrams the GSL appears to piggyback on the KSL phase, indicating that it is in fact of a descendant of the KSL

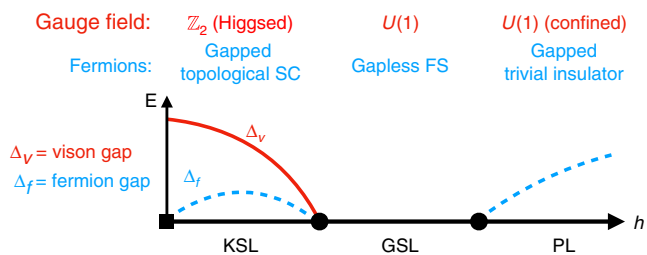


Fig. 7 Schematic phase diagram from the perspective of fermionic partons. The behavior of the fermions and associated gauge field indicated for the KSL, GSL, and PL phases. The flux (vicon) gap Δ_v and the fermion gap Δ_f is also shown

studies to further investigate the field theory description for this transition, which clearly lies beyond the standard Landau–Ginzburg–Wilson paradigm. Though current Kitaev materials are all believed to possess FM Kitaev couplings, the possibility of an AFM coupling is not ruled out on any microscopic grounds (early reports suggested that RuCl_3 possessed exactly such an AFM coupling) and indeed there is recent work suggesting that they may naturally appear in f -electron based systems⁴⁶. Future experimental studies on such Kitaev materials might be able to probe the nature of the fractional excitations in the gapless spin liquid regime and reveal the existence of a Fermi surface.

Note added: During the review process for this manuscript two preprints were posted^{47,48} that follow up on our work, providing further evidence that the intermediate phase is indeed a gapless $U(1)$ spin liquid with a spinon Fermi surface, as reported here.

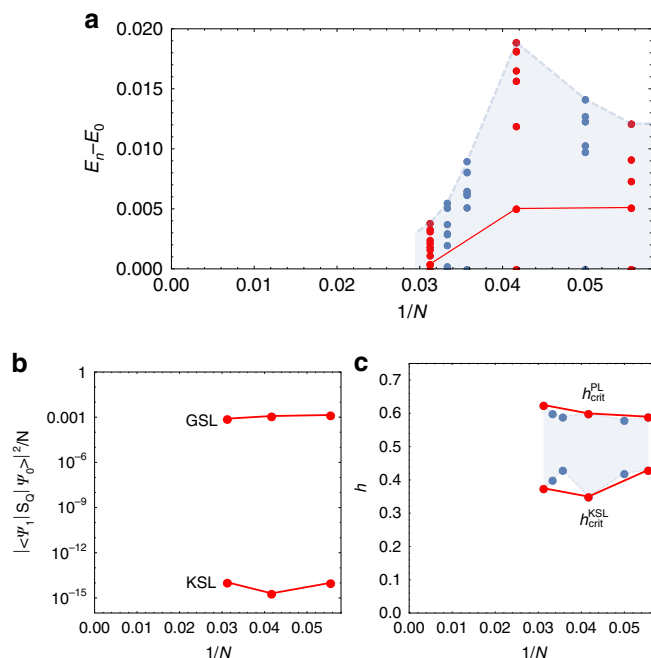


Fig. 8 Finite-size scaling. Shown, for a range of system sizes, are **a** the energy gaps between the ground state and the lowest lying state from each momentum sector for a point midway in the GSL phase, **b** the critical fields associated with the transition out of the KSL and into the PL phase, and **c** the spin spectral weight associated with the first excited state in the KSL and GSL phases. All data is taken along the cut corresponding to the upper of the two dashed lines (red) in Fig. 1a

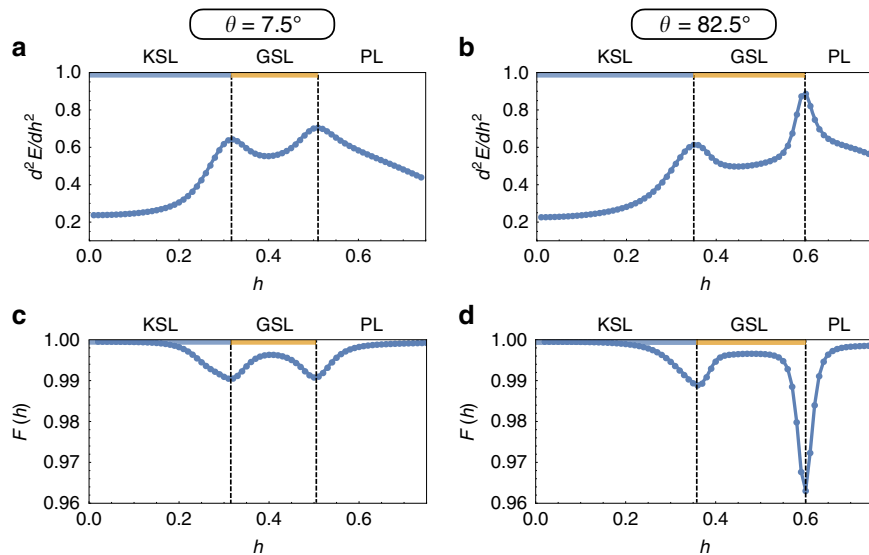


Fig. 9 Clear numerical signatures of phase transitions. In **a, b** the second derivative of the ground-state energy and **c, d** the ground-state fidelity is shown. These cuts correspond to the dashed lines (red) in Fig. 1a

Methods

Exact diagonalization and finite-size scaling. The exact diagonalization results were produced using the library ARPACK⁴⁹, primarily on an $N = 24$ site cluster with the full point group symmetry of the honeycomb lattice, and containing all the high-symmetry points of the Brillouin zone. Additional calculations were done on system sizes ranging from $N = 18$ to $N = 32$ sites, with qualitatively consistent results.

For a point midway in the GSL phase, we show in Fig. 8a the energy difference between the ground state and the lowest lying state from each momentum sector for $N = 18, 20, 24, 28, 30$, and 32 site clusters. The $N = 18, 24$, and 32 site clusters are highlighted in red as these are the only clusters that have the full point group symmetry of the honeycomb lattice. Unfortunately, unlike the $N = 24$ site system, the $N = 18$ and 32 site clusters do not contain all of the high-symmetry points in the BZ, marking out the $N = 24$ site cluster as unique and why we chose to show data for this cluster in the main manuscript. For the largest system sizes the density of states at low energies increases with increasing system size, with the largest gap for any momentum sector in the $N = 32$ site case being just $0.004K$. We also use a solid (red) line to indicate the gap to the first excited state for the symmetric clusters. The finite-size scaling is clear evidence that the intermediate phase is gapless, with an incredibly dense spectrum of excited states at low energies from all momentum sectors (for a detailed comparison to other ED studies see Supplementary Note 5).

We also show the spin spectral weight associated with the first excited state, $\sum_{\alpha} |\langle 1 | S_{\alpha}^z | 0 \rangle|^2$, in both the KSL and GSL phases for the three symmetric clusters in Fig. 8b (for the KSL we choose the first excited state above the ground state degenerate manifold). In the KSL phase, since all of the spectral weight is concentrated above the finite flux gap the weight associated to the first excited state is practically zero. On the other hand, at the same point midway in the GSL phase, the flux gap has collapsed to zero with the first excited state now showing finite spin spectral weight. This clearly demonstrates that the field-induced closure of the flux gap, via the transfer of spin spectral weight to zero energy, is a robust feature of the intermediate phase.

Finally we show the critical fields associated with the transition out of the KSL, $h_{\text{crit}}^{\text{KSL}}$, and the transition into the PL phase, $h_{\text{crit}}^{\text{PL}}$, in Fig. 8c. This clearly indicates that the intermediate phase is stable and its size is roughly $\sim 0.2K$ for the cut shown.

Determination of the phase boundaries. The phase boundaries for the phase diagrams presented in the main text were determined using a combination of the second derivative of the ground state energy and the ground-state fidelity, taken from a range of radial cuts (26 in angular spacings of $\pi/100$ and radial field spacing of $0.01/0.001$ for the AFM/FM cases, a total of 1976 points) for each of the three 2d phase diagrams presented in Figs. 1 and 2 (i.e., a total of 6000 parameter points were computed for each of Fig. 1a, b, Fig. 2a, b). For the ground-state energy, it is a peak in its second derivative which indicates the presence of a phase transition. The ground-state fidelity is defined as $F(g) = \langle \Psi_0(g) | \Psi_0(g + \delta g) \rangle$ for some tuning parameter g (in our case the magnitude of the magnetic field h). A first order transition, i.e., a level crossing, is signified by a discontinuity in the fidelity, while a second order transition results in a smooth dip. For the two cuts focused on in the main text, $\theta = 7.5^\circ$ and 82.5° in the c - b plane, we show in Fig. 9 these two quantities as a function of field magnitude. Two transitions can clearly be resolved,

with excellent agreement between the two distinct quantities. Finally, we note that we also find excellent agreement between the phase boundaries computed for our $N = 24$ site cluster and the phase boundaries reported in a recent infinite density matrix renormalization group study of the Kitaev model in a [111] magnetic field³².

Code availability. The code used to generate the data used in this study is available from the corresponding author upon reasonable request.

Data availability

The data that support the findings of this study are available from the corresponding author upon reasonable request.

Received: 21 May 2018 Accepted: 8 January 2019

Published online: 31 January 2019

References

- Savary, L. & Balents, L. Quantum spin liquids: a review. *Reports Progress. Phys.* **80**, 016502 (2017).
- Anderson, P. W. Resonating valence bonds: a new kind of insulator? *Mater. Res. Bull.* **8**, 153–160 (1973).
- Wen, X. Edge excitations in the fractional quantum hall states at general filling fractions. *Mod. Phys. Lett. B* **05**, 39–46 (1991).
- Abrikosov, A. A. Electron scattering on magnetic impurities in metals and anomalous resistivity effects. *Phys. Phys. Fiz.* **2**, 5–20 (1965).
- Tsvetlik, A. M. New fermionic description of quantum spin liquid state. *Phys. Rev. Lett.* **69**, 2142–2144 (1992).
- Kitaev, A. Anyons in an exactly solved model and beyond. *Anal. Phys.* **321**, 2–111 (2006).
- Read, N. & Sachdev, S. Large- n expansion for frustrated quantum antiferromagnets. *Phys. Rev. Lett.* **66**, 1773–1776 (1991).
- Senthil, T. & Fisher, M. P. A. Z_2 gauge theory of electron fractionalization in strongly correlated systems. *Phys. Rev. B* **62**, 7850–7881 (2000).
- Hermanns, M., Kimchi, I. & Knolle, J. Physics of the Kitaev model: fractionalization, dynamic correlations, and material connections. *Annu. Rev. Condens. Matter Phys.* **9**, 17–33 (2018).
- Khaliullin, G. Orbital order and fluctuations in Mott insulators. *Progress. Theor. Phys. Suppl.* **160**, 155–202 (2005).
- Jackeli, G. & Khaliullin, G. Mott insulators in the strong spin-orbit coupling limit: from Heisenberg to a quantum compass and Kitaev models. *Phys. Rev. Lett.* **102**, 017205 (2009).
- Trebst, S. Kitaev materials. Preprint at <http://arxiv.org/abs/arXiv:1701.07056> (2017).
- Chaloupka, J., Jackeli, G. & Khaliullin, G. Kitaev-Heisenberg model on a honeycomb lattice: possible exotic phases in iridium oxides $A_2\text{IrO}_3$. *Phys. Rev. Lett.* **105**, 027204 (2010).

14. Jiang, H.-C., Gu, Z.-C., Qi, X.-L. & Trebst, S. Possible proximity of the Mott insulating iridate Na_2IrO_3 to a topological phase: phase diagram of the Heisenberg-Kitaev model in a magnetic field. *Phys. Rev. B* **83**, 245104 (2011).
15. Kimchi, I. & You, Y.-Z. Kitaev-Heisenberg-J2-J3 model for the iridates A_2IrO_3 . *Phys. Rev. B* **84**, 180407 (2011).
16. Chaloupka, J., Jackeli, G. & Khaliullin, G. Zigzag magnetic order in the iridium oxide Na_2IrO_3 . *Phys. Rev. Lett.* **110**, 097204 (2013).
17. Rau, J. G., Lee, E. K.-H. & Kee, H.-Y. Generic spin model for the honeycomb iridates beyond the Kitaev limit. *Phys. Rev. Lett.* **112**, 077204 (2014).
18. Rousochatzakis, I., Reuther, J., Thomale, R., Rachel, S. & Perkins, N. B. Phase diagram and quantum order by disorder in the Kitaev K_1 - K_2 honeycomb magnet. *Phys. Rev. X* **5**, 041035 (2015).
19. Rau, J. G., Lee, E. K.-H. & Kee, H.-Y. Spin-orbit physics giving rise to novel phases in correlated systems: iridates and related materials. *Annu. Rev. Condens. Matter Phys.* **7**, 195–221 (2016).
20. Janssen, L., Andrade, E. C. & Vojta, M. Magnetization processes of zigzag states on the honeycomb lattice: identifying spin models for α - RuCl_3 and Na_2IrO_3 . *Phys. Rev. B* **96**, 064430 (2017).
21. Johnson, R. D. et al. Monoclinic crystal structure of α - RuCl_3 and the zigzag antiferromagnetic ground state. *Phys. Rev. B* **92**, 235119 (2015).
22. Kubota, Y., Tanaka, H., Ono, T., Narumi, Y. & Kindo, K. Successive magnetic phase transitions in α - RuCl_3 : XY-like frustrated magnet on the honeycomb lattice. *Phys. Rev. B* **91**, 094422 (2015).
23. Majumder, M. et al. Anisotropic $\text{Ru}^{3+} 4d^5$ magnetism in the α - RuCl_3 honeycomb system: susceptibility, specific heat, and zero-field NMR. *Phys. Rev. B* **91**, 180401 (2015).
24. Sears, J. A., Zhao, Y., Xu, Z., Lynn, J. W. & Kim, Y.-J. Phase diagram of α - RuCl_3 in an in-plane magnetic field. *Phys. Rev. B* **95**, 180411 (2017).
25. Hirobe, D., Sato, M., Shiom, Y., Tanaka, H. & Saitoh, E. Magnetic thermal conductivity far above the Neel temperature in the Kitaev-magnet candidate α - RuCl_3 . *Phys. Rev. B* **95**, 241112 (2017).
26. Kasahara, Y. et al. Unusual thermal hall effect in a Kitaev spin liquid candidate α - RuCl_3 . *Phys. Rev. Lett.* **120**, 217205 (2018).
27. Arnab, B. et al. Excitations in the field-induced quantum spin liquid state of α - RuCl_3 . *npj Quantum Mater.* **3**, 8 (2018).
28. Nejc, J. et al. Observation of two types of fractional excitation in the Kitaev honeycomb magnet. *Nat. Phys.* **14**, 786–790 (2018).
29. Kasahara, Y. et al. Majorana quantization and half-integer thermal quantum Hall effect in a Kitaev spin liquid. *Nature* **559**, 227–231 (2018).
30. Fey, S. Field-driven instabilities of the non-abelian topological phase in the Kitaev model. MSc Thesis, Technische Universität Dortmund (2013).
31. Zhu, Z., Kimchi, I., Sheng, D. N. & Fu, L. Robust non-Abelian spin liquid and a possible intermediate phase in the antiferromagnetic Kitaev model with magnetic field. *Phys. Rev. B* **97**, 241110 (2018).
32. Gohlke, M., Moessner, R. & Pollmann, F. Dynamical and topological properties of the Kitaev model in a [111] magnetic field. *Phys. Rev. B* **98**, 014418 (2018).
33. Zhang, Y., Grover, T., Turner, A., Oshikawa, M. & Vishwanath, A. Quasiparticle statistics and braiding from ground-state entanglement. *Phys. Rev. B* **85**, 235151 (2012).
34. O'Brien, K., Hermanns, M. & Trebst, S. Classification of gapless spin liquids in three-dimensional Kitaev models. *Phys. Rev. B* **93**, 085101 (2016).
35. Knolle, J., Kovrizhin, D. L., Chalker, J. T. & Moessner, R. Dynamics of a two-dimensional quantum spin liquid: signatures of emergent majorana fermions and fluxes. *Phys. Rev. Lett.* **112**, 207203 (2014).
36. Knolle, J., Kovrizhin, D. L., Chalker, J. T. & Moessner, R. Dynamics of fractionalization in quantum spin liquids. *Phys. Rev. B* **92**, 115127 (2015).
37. Sugiura, S. & Shimizu, A. Thermal pure quantum states at finite temperature. *Phys. Rev. Lett.* **108**, 240401 (2012).
38. Sugiura, S. & Shimizu, A. Canonical thermal pure quantum state. *Phys. Rev. Lett.* **111**, 010401 (2013).
39. Nasu, J., Udagawa, M. & Motome, Y. Vaporization of Kitaev spin liquids. *Phys. Rev. Lett.* **113**, 197205 (2014).
40. Metlitski, M. A., Mross, D. F., Sachdev, S. & Senthil, T. Cooper pairing in non-Fermi liquids. *Phys. Rev. B* **91**, 115111 (2015).
41. Galitski, V. & Kim, Y. B. Spin-triplet pairing instability of the spinon Fermi surface in a $U(1)$ spin liquid. *Phys. Rev. Lett.* **99**, 266403 (2007).
42. Burnell, F. J. & Nayak, C. $SU(2)$ slave fermion solution of the Kitaev honeycomb lattice model. *Phys. Rev. B* **84**, 125125 (2011).
43. Lai, H.-H. & Motrunich, O. I. $SU(2)$ -invariant Majorana spin liquid with stable parton Fermi surfaces in an exactly solvable model. *Phys. Rev. B* **84**, 085141 (2011).
44. Lahtinen, V., Ludwig, A. W. W., Pachos, J. K. & Trebst, S. Topological liquid nucleation induced by vortex-vortex interactions in Kitaev's honeycomb model. *Phys. Rev. B* **86**, 075115 (2012).
45. Lahtinen, V., Ludwig, A. W. W. & Trebst, S. Perturbed vortex lattices and the stability of nucleated topological phases. *Phys. Rev. B* **89**, 085121 (2014).
46. Jang, S.-H., Sano, R., Kato, Y. & Motome, Y. Antiferromagnetic Kitaev interaction in f-electron based honeycomb magnets. Preprint at <https://arxiv.org/abs/1807.01443> (2018).
47. Jiang, H.-C., Wang, C.-Y., Huang, B. & Lu, Y.-M. Field induced quantum spin liquid with spinon Fermi surfaces in the Kitaev model. Preprint at <https://arxiv.org/abs/1809.08247> (2018).
48. Zou, L. & He, Y.-C. Field-induced neutral Fermi surface and QCD₃-Chern-Simons quantum criticalities in Kitaev materials. Preprint at <https://arxiv.org/abs/1809.09091> (2018).
49. Lehoucq, R. B., Sorensen, D. C. & Yang, C. *ARPACK Users Guide: Solution of Large Scale Eigenvalue Problems by Implicitly Restarted Arnoldi Methods* (SIAM, 1997).
50. Polyakov, A. M. Quark confinement and topology of gauge theories. *Nuclear Physics B* **120**, 429–458 (1977).

Acknowledgements

We thank A. Rosch for useful discussions. This work was supported by the Deutsche Forschungsgemeinschaft (DFG, German Research Foundation)—Projektnummer 277101999—TRR 183 (project B01). The numerical simulations were performed on the CHEOPS cluster at RRZK Cologne and the JUWELS cluster at FZ Jülich.

Author contributions

C.H. carried out the numerical simulations and analyzed the data. Both authors contributed to the interpretation of results and jointly wrote the manuscript.

Additional information

Supplementary Information accompanies this paper at <https://doi.org/10.1038/s41467-019-08459-9>.

Competing interests: The authors declare no competing interests.

Reprints and permission information is available online at <http://npj.nature.com/reprintsandpermissions/>

Journal peer review information: *Nature Communications* thanks the anonymous reviewers for their contribution to the peer review of this work.

Publisher's note: Springer Nature remains neutral with regard to jurisdictional claims in published maps and institutional affiliations.

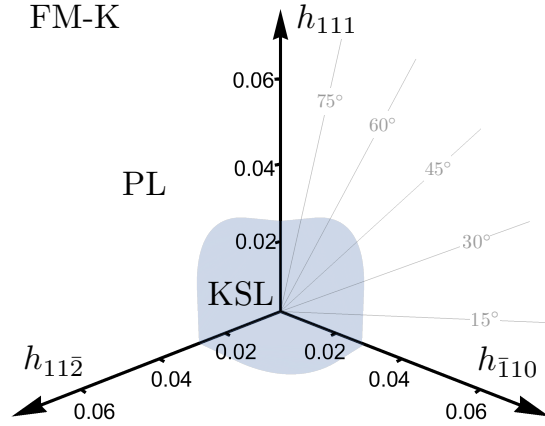


Open Access This article is licensed under a Creative Commons Attribution 4.0 International License, which permits use, sharing, adaptation, distribution and reproduction in any medium or format, as long as you give appropriate credit to the original author(s) and the source, provide a link to the Creative Commons license, and indicate if changes were made. The images or other third party material in this article are included in the article's Creative Commons license, unless indicated otherwise in a credit line to the material. If material is not included in the article's Creative Commons license and your intended use is not permitted by statutory regulation or exceeds the permitted use, you will need to obtain permission directly from the copyright holder. To view a copy of this license, visit <http://creativecommons.org/licenses/by/4.0/>.

© The Author(s) 2019

Supplementary Information
Emergence of a Field-Driven $U(1)$ Spin Liquid in the Kitaev Honeycomb Model

Ciarán Hickey and Simon Trebst
Institute for Theoretical Physics, University of Cologne, 50937 Cologne, Germany



Supplementary Figure 1. Phase diagram in uniform magnetic field. For the pure FM Kitaev model, shown here, there are just two phases, the KSL and PL phases, and a single transition between them.

SUPPLEMENTARY NOTE 1: FERROMAGNETIC KITAEV PHASE DIAGRAM

For ferromagnetic Kitaev exchange the phase diagram in tilted magnetic fields exhibits just two phases, the gapped KSL and the trivial PL phase. The phase diagram is shown in the main text in Fig. 1(b). In Supplementary Figure 1 we provide the same phase diagram, but with the axes scales reduced by an order of magnitude so as to make the boundaries of the KSL phase more visible.

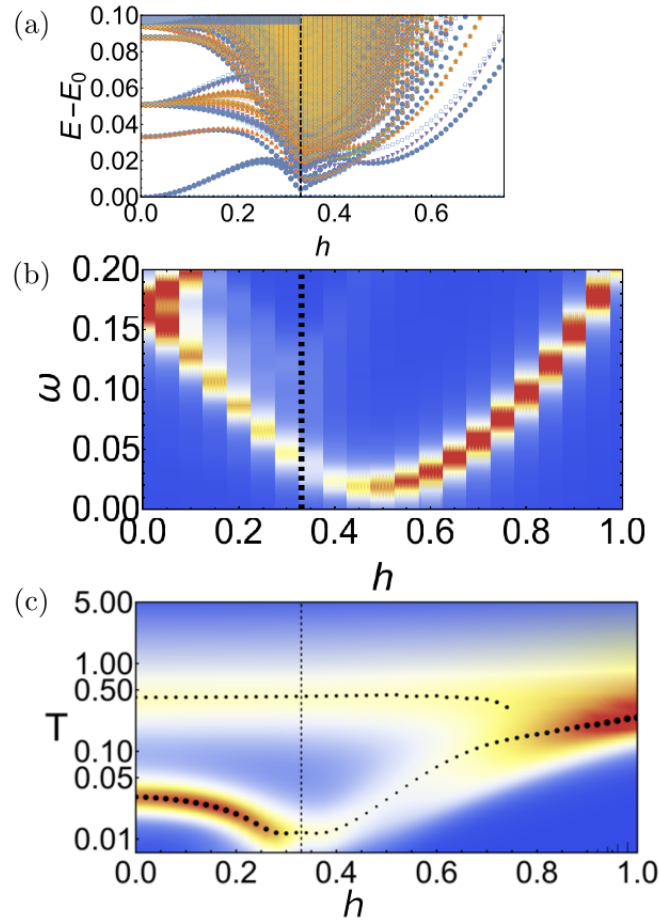
SUPPLEMENTARY NOTE 2: DIRECT KSL-PL TRANSITION

Along certain field directions there is a direct transition from the KSL to the PL phase, with no intermediate GSL phase. In Supplementary Figure 2 we show a selection of data for such a scenario. In particular we take a cut at 30° away from the $[\bar{1}10]$ direction, within the honeycomb plane, toward the $[111]$ direction, perpendicular to the plane. We show the energy spectrum, the dynamical structure factor for the Γ' point and the specific heat as a function of increasing field magnitude.

SUPPLEMENTARY NOTE 3: DYNAMICAL STRUCTURE FACTOR

In the main text, it has been argued that the flux gap at zero field breaks apart and moves to lower energy as the external magnetic field is increased, eventually closing fully as the transition to the GSL is crossed. As an example we showcased, in Fig. 4(d) of the main manuscript, the intensity at the Γ' point as a function of field magnitude, with two transitions clearly visible as the spin gap closes at the KSL-GSL transition, remains closed throughout the GSL phase, and then reopens again at the GSL-PL transition. Here we show similar plots for other high-symmetry points, namely examples of M , X and K points. At all of these momenta the same trend is undoubtedly present, with the flux gap at zero field being broken apart and physical spin spectral weight being pushed down to zero energy as the GSL is entered.

However we note that, depending on the field direction, this trend may not be true for all momenta. In particular, if the field along a particular spin axis is negligible, the points in momentum space associated with the corresponding spin component will not be as strongly affected (as spin and momentum space are intrinsically linked together in the Kitaev model, for example the bond in real space associated with say the x -component of the spin translates into a particular direction in the BZ). As a result the flux gap will only fully collapse for those momenta along which the corresponding field magnitude is large. An example of this is shown in Fig. Supplementary Figure 4 where we plot the dynamical spin structure factor in the middle of the GSL along the cut at $\theta = 7.5^\circ$ away from the $[\bar{1}10]$ axis. In this case the field along the z -axis, h_z , is much smaller compared to the other two components. This results in the flux gap remaining mostly intact at, say, X_1 and K_1 for example, while it closes at the remaining momenta. This raises the interesting possibility that the gauge field excitations may be anisotropic. In other words the gauge field propagator may be gapless for excitations with \vec{k} along certain directions, and gapped for other directions, which could be captured by a \vec{k} -dependent mass.



Supplementary Figure 2. Direct KSL to PL transition. Data with (a) the energy spectrum, (b) the dynamical spin structure factor at the Γ' point, and (c) the specific heat shown for a cut 30° away from $[\bar{1}10]$ toward $[111]$.

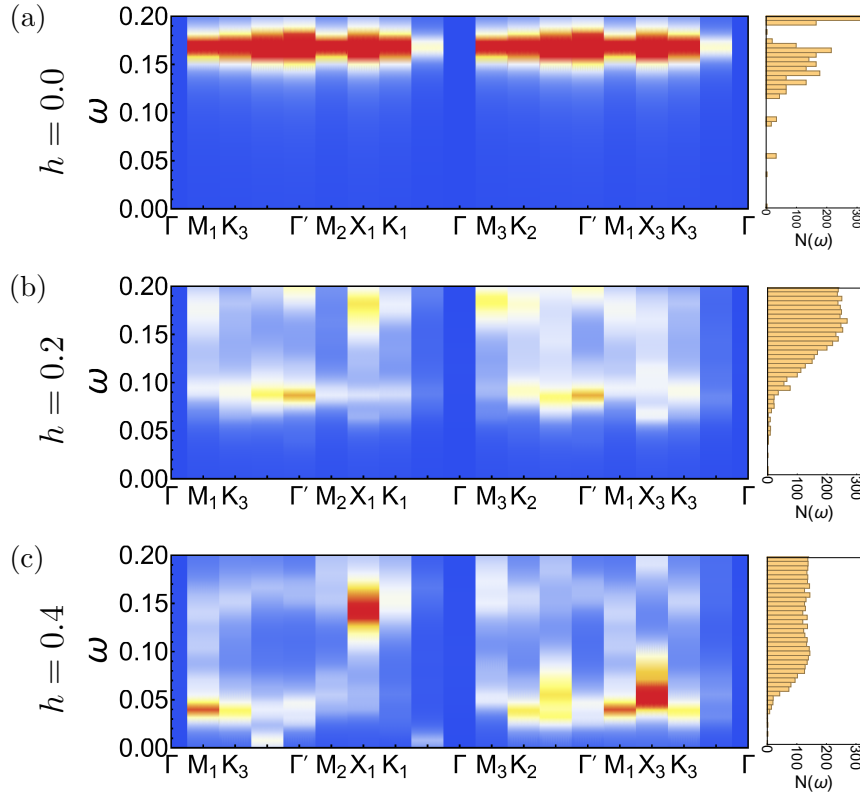
SUPPLEMENTARY NOTE 4: STABILITY OF THE FERMI SURFACE

Regarding the stability of the Fermi surface, though a normal Fermi liquid is unstable to an infinitesimal attractive interaction, coupling to a dynamical $U(1)$ gauge field stabilizes the Fermi surface up to a finite critical strength of the interaction [1]. Further, we note that while there are several symmetry-allowed fermionic pairing terms, these will carry a non-trivial momentum dependence due to the shift of the Dirac cone away from high-symmetry momenta for generic field directions and as such will not contribute to the low-energy sector, as at least one of the momenta is far away from the Fermi surface. Note, however, that for magnetic fields applied along high-symmetry directions, some of these pairing terms might become relevant and thereby lead to a spin-Peierls instability akin to what has been discussed for Majorana Fermi surfaces [2].

SUPPLEMENTARY NOTE 5: EXACT DIAGONALIZATION RESULTS IN CONTEXT

For those that may not necessarily be familiar with the energy scales typically encountered in exact diagonalization (ED) studies we would like to highlight the smallness of the gaps encountered in this work when compared to some known ED results. In particular we can compare to:

- The regular Heisenberg antiferromagnet on square, triangular and honeycomb lattices. In all cases the ground state is magnetically ordered with gapless Goldstone modes. Examples of spin gaps from ED include, $\Delta = 0.288$ for an $N = 36$ site symmetric square cluster, $\Delta = 0.123$ for an $N = 36$ site symmetric triangular cluster and $\Delta = 0.214$ for an $N = 32$ site symmetric honeycomb cluster. Even the reported extrapolated gaps, taken from considering a range of system sizes, are much larger than those in the GSL (for all cluster sizes we have studied), being $\Delta_\infty = 0.025$ for the square lattice (taken from 12 lattices ranging from $N = 18 - 40$), $\Delta_\infty = 0.129$ for the triangular lattice (taken from 12 lattices ranging

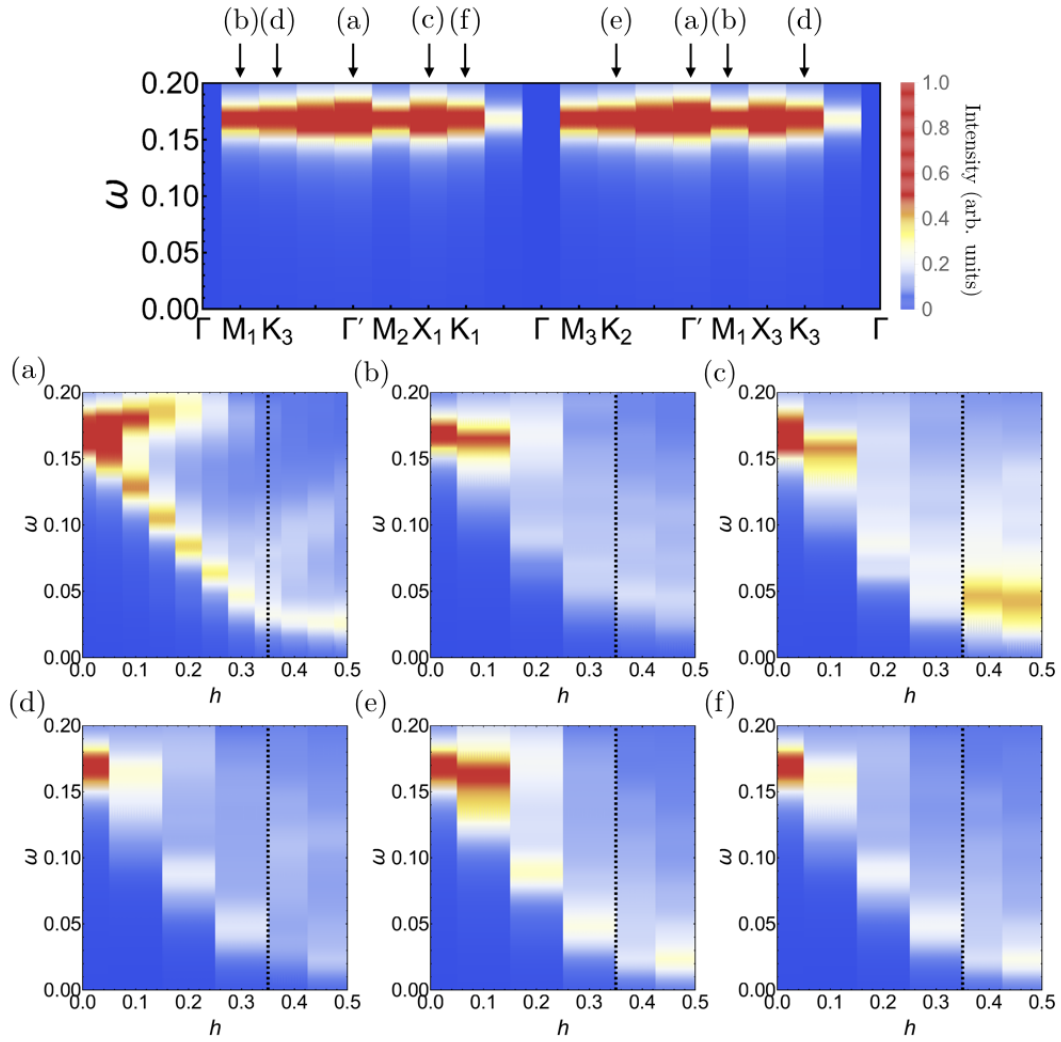


Supplementary Figure 3. Dynamical spin structure factor. (a) The zero-field KSL, (b) a point midway in the KSL phase and (c) a point in the middle of the GSL along a path through all high-symmetry points of the extended Brillouin zone for the cut $\theta = 7.5^\circ$, the lower of the two dashed red lines in Fig. 1(c) of the main text.

from $N = 24 - 36$) and $\Delta_\infty = 0.050$ for the honeycomb lattice (taken from 14 lattices ranging from $N = 6 - 38$). All values are taken from [3] and references therein.

- The Kagome lattice Heisenberg antiferromagnet (KHAFM). There is an ongoing debate as to whether this is a gapless Dirac spin liquid or a gapped \mathbb{Z}_2 spin liquid. In either case the gap between the ground state and first excited state should go to zero for a torus geometry (for the Dirac SL because it is gapless and for the \mathbb{Z}_2 QSL because there should be a four-fold ground state degeneracy). A recent ED study has investigated $N = 36, 42$ and 48 site clusters [4]. The encountered gaps are $\Delta = 0.010, 0.020$ and 0.021 , respectively. In other words, if we take the smallest ED gap for the KHAFM (the $N = 36$ site cluster), then we can fit the lowest lying state from every single momentum sector within this gap for our $N = 30$ and 32 site clusters. If we take the ED gap from the largest system size studied, the $N = 48$ site cluster, then for all of our clusters, $N = 18 - 32$ sites, we can fit the lowest lying state from every single momentum sector within this gap.
- Recent studies of Kalmeyer-Laughlin chiral spin liquids. Such phases have a two-fold degenerate ground state manifold (GSM) for a toroidal geometry which is exponentially split on finite sized systems, meaning the gap between the ground state and first excited state should scale to zero. As a particularly enlightening comparison we can compare our $N = 32$ site honeycomb results with results for CSLs on $N = 32$ site honeycomb lattices. Comparing to data from [5] and [6] they find gaps of $\Delta = 0.011$ and $\Delta = 0.035$ respectively. For our $N = 32$ site results we can again fit at least 16 states (one from each momentum sector) within these gaps.

In summary, when compared to other ED studies for states, which we either know to be gapless or know/suspect to have a ground state degeneracy, the gaps encountered in our study are exceptionally small, not just for the first excited state but for the lowest lying state in every single momentum sector.



Supplementary Figure 4. Dynamical spin structure factor at various high-symmetry points. (a) Γ' , (b) one of the M points, (c) one of the X points, and (d)-(f) the three distinct K points. The intensity is shown as a function of increasing field along the cut $\theta = 82.5^\circ$, the upper of the two dashed red lines in Fig. 1(c) of the main text.

-
- [1] M. A. Metlitski, D. F. Mross, S. Sachdev, and T. Senthil, *Phys. Rev. B* **91**, 115111 (2015).
 - [2] M. Hermanns, S. Trebst, and A. Rosch, *Phys. Rev. Lett.* **115**, 177205 (2015).
 - [3] J. Richter, J. Schulenburg, and A. Honecker, “Quantum magnetism in two dimensions: From semi-classical néel order to magnetic disorder,” in *Quantum Magnetism*, edited by U. Schollwöck, J. Richter, D. J. J. Farnell, and R. F. Bishop (Springer Berlin Heidelberg, Berlin, Heidelberg, 2004) pp. 85–153.
 - [4] A. M. Läuchli, J. Sudan, and R. Moessner, Preprint at <https://arxiv.org/abs/1611.06990> (2016).
 - [5] Y.-F. Wang, H. Yao, Z.-C. Gu, C.-D. Gong, and D. N. Sheng, *Phys. Rev. Lett.* **108**, 126805 (2012).
 - [6] C. Hickey, L. Cincio, Z. Papić, and A. Paramekanti, *Phys. Rev. Lett.* **116**, 137202 (2016).